2004

Metallic single-walled silicon nanotubes

Jaeil Bai
University of Nebraska-Lincoln

Xiao Cheng Zeng
University of Nebraska-Lincoln, xzeng1@unl.edu

Hideki Tanaka
Okayama University, htanakaa@cc.okayama-u.ac.jp

J. Y. Zeng
Peking University

Metallic single-walled silicon nanotubes

Jaeil Bai*, X. C. Zeng*†, Hideki Tanaka‡, and J. Y. Zeng§

*Departments of Chemistry and Physics, University of Nebraska, Lincoln, NE 68588; ‡Department of Chemistry, Okayama University, Okayama 700-8530, Japan; and §Department of Physics, Peking University, Beijing 100871, China

Communicated by Howard Reiss, University of California, Los Angeles, CA, December 18, 2003 (received for review July 10, 2003)

Atomistic computer-simulation evidences are presented for the possible existence of one-dimensional silicon nanostructures: the square, pentagonal, and hexagonal single-walled silicon nanotubes (SWSNTs). The local geometric structure of the SWSNTs differs from the local tetrahedral structure of cubic diamond silicon, although the coordination number of atoms of the SWSNTs is still fourfold. *Ab initio* calculations show that the SWSNTs are locally stable in vacuum and have zero band gap, suggesting that the SWSNTs are possibly metals rather than wide-gap semiconductors.

Low-dimensional nanostructures are known to have properties that can be markedly different from their bulk counterparts. For example, as shown in a recent experiment (1), Ho and coworkers demonstrated atom-by-atom evolution of electronic band structure of 1D gold chain. For semiconductor nanostructures, when the carriers (electrons and holes) are confined to dimensions less than their de Bröglie wavelength (typically a few nanometers), quantum-mechanical size effects can emerge. The carrier confinement at the nanoscale can be in 0D (quantum dots), 1D (quantum wires), or 2D (quantum wells) (2). Indeed, the current interest in fabricating low-dimensional semiconductor nanostructures, coined as band-structure engineering, has largely relied on novel quantum-mechanical size effects.

The crystalline structure of 3D bulk silicon is cubic diamond, similar to that of carbon diamond. However, unlike the carbon counterpart (3), a 1D single-walled silicon nanotube (SWSNT) has not been found in nature yet, largely because silicon prefers sp^3 bonds rather than sp^2 bonds (4). Indeed, silicon has been viewed as nontubular solid rather than tubular solid, similar to carbon and boron nitride. The cubic diamond silicon is known as a semiconductor with an energy band gap of 1.17 eV (1 eV = 1.602×10^{-19} J). At high pressures, however, the cubic-diamond-structured silicon can undergo a phase transformation to highly coordinated (sixfold or above) metallic phases such as the β-tin and hexagonal closed-packed structures (5). To date, experimentally produced 1D-like nanostructures of silicon [e.g., porous silicon (6) and silicon nanowires (7–12)] all assume either the cubic diamond crystalline structure or the local structure of amorphous silicon. A commonly reported electronic property of the 1D silicon nanostructures is that they all have wider band gap than the cubic diamond silicon. Here we present atomistic computer-simulation evidences of three thinnest SWSNTs: the square, pentagonal, and hexagonal silicon nanotubes. The local geometric structure of these SWSNTs differs from that of cubic diamond silicon and the surface-passivated 1D silicon nanowires. It also differs from that of the carbon-nanotube-like "hypothetical" SWSNTs (4, 13–15), because the latter types of SWSNTs are composed of both sp^3 and sp^2 bonds. Moreover, *ab initio* quantum-mechanical calculations show that the present SWSNTs exhibit an entirely opposite trend in the band-gap change compared with the 1D silicon nanowires. Consequently, the SWSNTs are likely metals rather than wide-gap semiconductors.

Preliminary evidence for the existence of 1D SWSNTs was derived from the classical molecular dynamics (MD) simulation of confined molten silicon within a cylindrical nanopore. We used the Stillinger–Weber potential for the bulk silicon (16), which is known to yield nearly the same melting point (1691 K) as the measurement (1683 K) (17, 18). The model nanopore is merely to provide a chemically inert confinement for the molten silicon. For this purpose, we simply used a structureless infinite Lennard–Jones nanopore. The potential function of the nanopore is the Lennard–Jones integrated over the cylindrical area of the nanopore with Steele's potential parameters for graphite (19). The diameter of the nanopore ranges from 8.98 to 10.86 Å. We carried out constant-temperature and axial-pressure (the pressure tensor in the axial direction was set at 200 MPa) MD simulation by using Nosé–Andersen's method (20). The simulation cell contains 120 Si atoms. The periodic boundary condition was applied in the axial direction. The temperature was lowered in step from 2503 toward 1633 K and then raised back to >2000 K. At each given temperature, 5–20 million MD time steps (each MD time step is 0.3 fs) were used for the equilibration, and thereafter the instantaneous configurations of the system were mapped onto corresponding potential-energy local-minimum configurations by using the constant-volume steepest-descent method. The minimized energy, excluding the interaction energy between silicon and the nanopore, is denoted as the quenched potential energy of the confined system.

Fig. 1*A* displays the quenched potential energy versus temperature. It shows that the quenched potential energy exhibits an abrupt drop on cooling and jump on heating. This marked hysteresis-loop behavior evinces a first-order phase transition for the confined silicon within the nanopore. In the 10.65-Å-diameter nanopore, the lower temperature phase is found to be a hexagonal SWSNT (Fig. 1*B*). At 1877 K, we find that the diffusion constant (along the axial direction) is $<10^{-8}$ cm^2·s^{-1}, indicating that the hexagonal SWSNT is solid-like. In the 9.82- and 8.98-Å-diameter nanopores, the observed low-temperature solid-like phase is a pentagonal and square SWSNT, respectively (Fig. 1 *C* and *D*). Note that the geometric structure of these SWSNTs resembles that of the hydrogen-bonding network of 1D ice nanotubes (21).

Because the initial evidence for the existence of SWSNTs was obtained from the classical MD simulation with the empirical Stillinger–Weber potential (developed to fit bulk properties of silicon), questions may arise regarding whether the potential function is applicable for silicon in the highly confined environment or whether this evidence is an artifact of the empirical potential. To confirm that the 1D SWSNTs seen in the MD simulation are indeed a stable allotropic form of silicon, we first examined local stability of a finite-size stacked-pentagon silicon cluster terminated by hydrogen atoms at the ends, that is, $Si_{5n}H_{10}$ (n = 3, 4, 5, 8) (Fig. 2). This is because the bonding feature of the $Si_{5n}H_{10}$ (n is an integer) clusters is very similar to that of the infinite SWSNTs; namely, the coordination number of every Si atom (except those at the ends) is fourfold. Note that previous *ab initio* calculations have shown that small-sized silicon clusters tend to favor a higher coordination number than fourfold

Abbreviations: SWSNT, single-walled silicon nanotube; MD, molecular dynamics; B3LYP, Becke's three-parameter and Lee–Yang–Parr correlation functionals; DFT, density-functional theory; MP2, Møller–Plesset perturbation theory of second order; HOMO, highest occupied molecular orbital; LUMO, lowest unoccupied molecular orbital; DOS, density of states.

†To whom correspondence should be addressed. E-mail: xczeng@phase1.unl.edu.

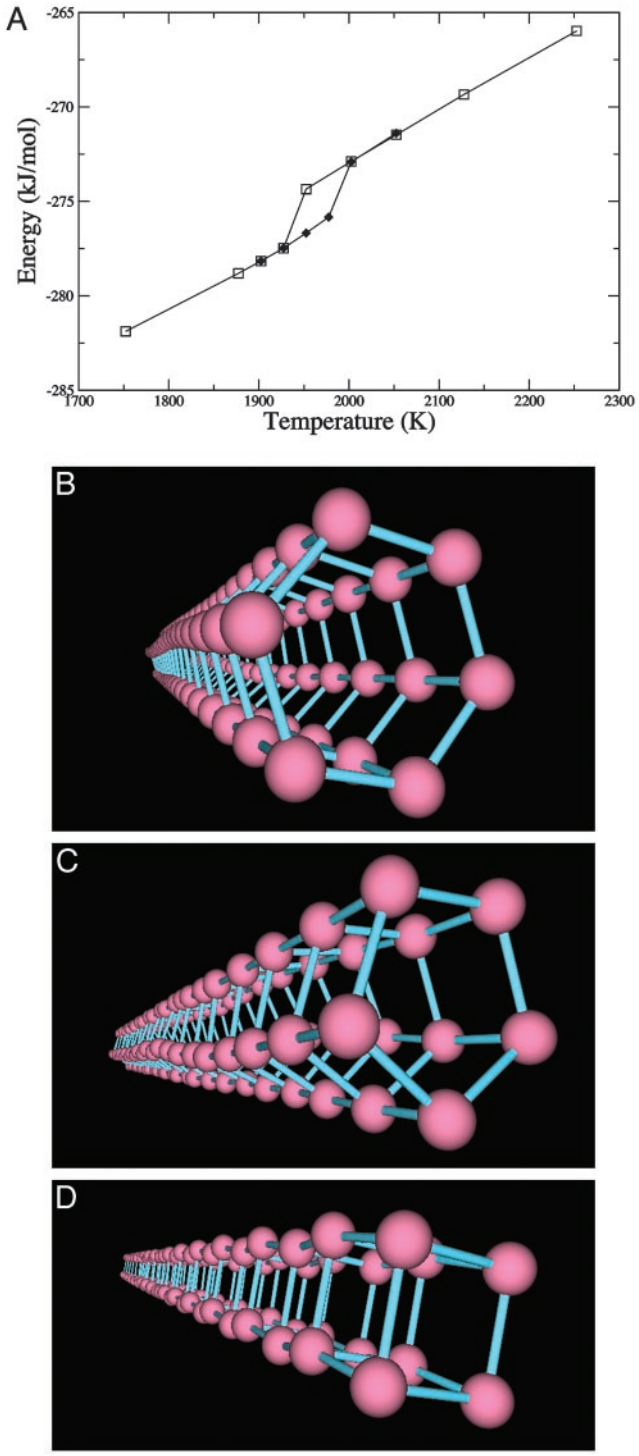

Fig. 1. (*A*) Quenched potential energy (excluding nanopore–Si interaction) versus temperature for the confined silicon inside a Lennard–Jones nanopore with a diameter of 10.62 Å. Open and filled symbols denote the cooling and heating process, respectively. (*B–D*) Snapshots of quenched structure of the hexagonal (*B*), pentagonal (*C*), and square (*D*) SWSNTs.

(22–24). Hence, without the hydrogen termination at the ends, the stacked-pentagon silicon clusters will be unstable.

The geometries of the four clusters were optimized at the all-electron Becke's three-parameter and Lee–Yang–Parr correlation functionals (B3LYP)/6-31G(d) level of density-functional theory (DFT) (25). Harmonic vibrational analysis at

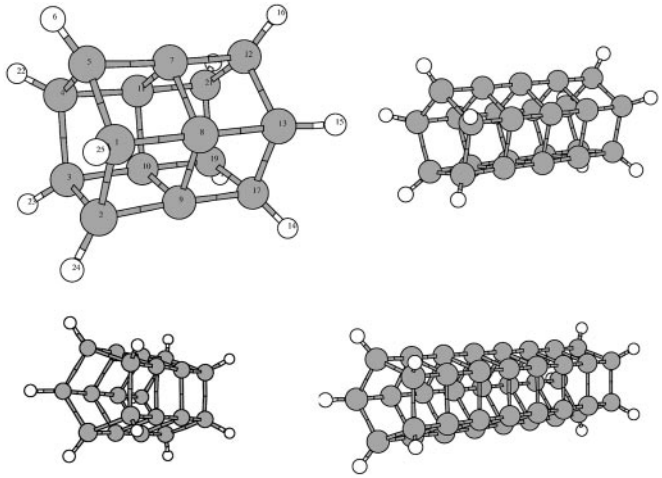

Fig. 2. Stacked-pentagon clusters $Si_{5n}H_{10}$ ($n = 3, 4, 5, 8$). Gray spheres are Si atoms, and white spheres are H atoms. The point-group symmetry of the clusters is D_{5h}.

the same level was performed to assure that the optimized clusters are stable. In addition, for the two smaller clusters, the geometric structures were also optimized at the Møller–Plesset

Table 1. Si–Si bond distance (Å) for cluster $Si_{15}H_{10}$ calculated at the MP2/6-31G(d) level of theory

Bond	Distance, Å
Si_1–Si_2	2.4151
Si_1–Si_5	2.4151
Si_1–Si_8	2.3791
Si_1–H_{25}	1.4973
Si_2–Si_3	2.4151
Si_2–Si_9	2.3791
Si_2–H_{24}	1.4973
Si_3–Si_3	2.4151
Si_3–Si_{10}	2.3791
Si_3–H_{23}	1.4973
Si_4–Si_5	2.4151
Si_4–Si_{11}	2.3791
Si_4–H_{22}	1.4973
Si_5–H_6	1.4973
Si_5–Si_7	2.3791
Si_7–Si_8	2.3336
Si_7–Si_{11}	2.3336
Si_7–Si_{12}	2.3788
Si_8–Si_9	2.3336
Si_8–Si_{13}	2.3788
Si_9–Si_{10}	2.3336
Si_9–Si_{17}	2.3788
Si_{10}–Si_{11}	2.3336
Si_{10}–Si_{19}	2.3788
Si_{11}–Si_{21}	2.3788
Si_{12}–Si_{13}	2.4148
Si_{12}–H_{16}	1.498
Si_{12}–Si_{21}	2.4148
Si_{13}–H_{15}	1.498
Si_{13}–Si_{17}	2.4148
H_{14}–Si_{17}	1.498
Si_{17}–Si_{19}	2.4148
H_{18}–Si_{19}	1.498
Si_{19}–Si_{21}	2.4148
H_{20}–Si_{21}	1.498

Table 2. Single-point energy and HOMO–LUMO gap calculated at the B3LYP/6-31G(d) level for clusters $Si_{5n}H_{10}$ (n = 3, 4, 5, 8) and single-point energy calculated at the MP2/6-31G(d) level for clusters $Si_{5n}H_{10}$ (n = 3, 4)

Cluster	Energy (Hartree)	Energy (Hartree)	HOMO-LUMO gap, eV
$Si_{15}H_{10}$	−4348.404087	−4340.7459234	2.263
$Si_{20}H_{10}$	−5795.8483941	−5785.7223773	1.512
$Si_{25}H_{10}$	−7243.3072149	—	1.445
$Si_{40}H_{10}$	−11585.6609068	—	0.888

perturbation theory of second order (MP2)/6-31G(d) level of molecular-orbital theory. The calculated geometric parameters [at the MP2/6-31G(d) level] for the smallest cluster is given in Table 1. Table 2 gives the calculated energies at the B3LYP/6-31G(d) and MP2/6-31G(d) levels, as well as the highest occupied molecular orbital (HOMO)-lowest unoccupied molecular orbital (LUMO) gaps at the B3LYP/6-31G(d) level. We noticed that the HOMO–LUMO gap decreases appreciably as the number of pentagons increases in the clusters. Table 3 lists the calculated vibrational frequencies and the associated IR intensities at the B3LYP/6-31G(d) level. No imaginary frequencies were found for all four clusters.

The fact that the finite-size $Si_{5n}H_{10}$ clusters are locally stable and that the HOMO–LUMO gap decreases with the increasing size of the clusters prompts us to examine further the local stability of the infinite stacked-polygon silicon nanotubes (i.e., the pentagonal SWSNT) and their band gaps by means of *ab initio* calculations. Toward this end, we used the plane-wave-based DFT within the Perdew–Wang generalized gradient approximation (26), which is implemented in the CASTEP computer code (Accelyrs Inc., San Diego) (27). The wave functions were expanded in terms of a plane-wave basis set with a kinetic energy cutoff of 180 eV. The ion–valence electron interactions were represented by ultrasoft pseudopotential (28). The Brillouin zone was sampled with $(1 \times 1 \times 5)k$ points of a Monkhorst–Pack grid (29). The supercell geometry was taken to be a tetragonal cell with the dimension $L \times L \times L_z$, where the z direction is defined as the axial direction of the nanotubes. In the *ab initio* calculations, L was fixed at 50 Å, whereas the initial value of L_z was set at 4.8 Å, twice the mean interlayer distance for the $Si_{40}H_{10}$ cluster. During the geometry relaxation, only L_z varies to

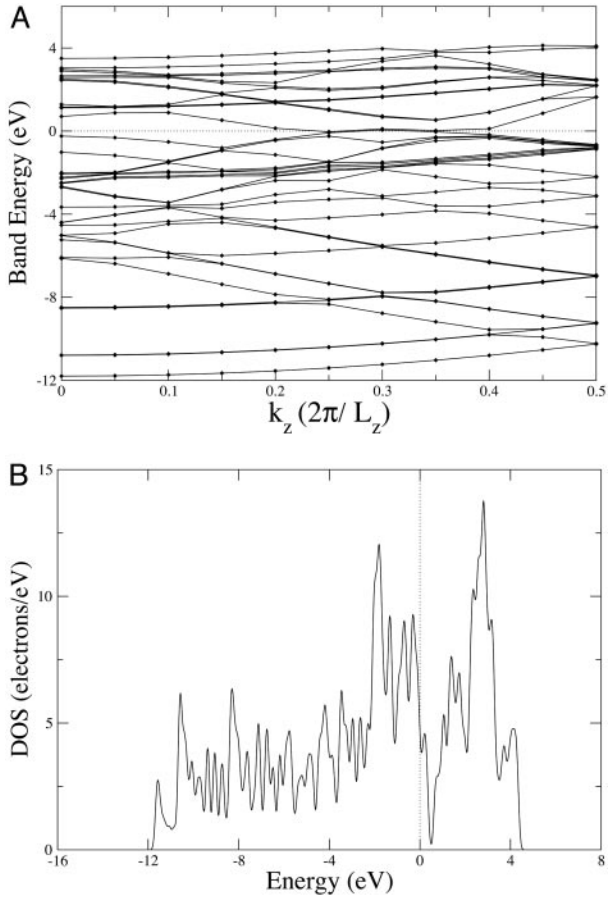

Fig. 3. (*A*) Electronic band structure of the hexagonal SWSNT (the Fermi energy is set to zero). (*B*) The electronic DOS of the hexagonal SWSNT.

Table 3. Vibrational frequency (cm^{-1}) and IR intensity (in parentheses) calculated at the B3LYP/6-31G(d) level for the clusters $Si_{5n}H_{10}$ (n = 3, 4, 5)

Cluster	Frequency (intensity)			
$Si_{15}H_{10}$	118.75 (2.84)	271.13 (0.85)	353.30 (0.97)	486.87 (0.52)
	567.47 (10.25)	590.83 (130.26)	659.43 (99.41)	2167.06 (3.36)
	2168.62 (630.95)	2173.42 (1173.36)	2178.59 (0.52)	
$Si_{20}H_{10}$	91.29 (1.19)	92.20 (1.20)	216.07 (0.13)	216.4 (0.12)
	317.48 (8.91)	350.90 (8.83)	351.80 (0.84)	363.01 (0.78)
	382.07 (6.78)	540.45 (4.35)	541.10 (1.92)	542.28 (2.70)
	581.64 (133.61)	582.05 (0.75)	583.95 (4.02)	584.36 (23.35)
	588.82 (0.88)	590.74 (2.32)	646.24 (79.62)	646.72 (79.5)
	2167.83 (23.16)	2160.05 (17.47)	2168.90 (0.14)	2169.08 (36.11)
	2173.90 (1.64)	2174.22 (524.65)	2175.38 (30.12)	2175.73 (563.85)
	2179.95 (1404.82)	2183.65 (5.04)		
$Si_{25}H_{10}$	73.37 (0.56)	73.98 (0.55)	108.24 (2.04)	193.62 (0.50)
	193.62 (0.49)	194.00 (0.49)	309.65 (27.45)	326.48 (2.01)
	348.00 (4.50)	355.25 (1.15)	355.98 (1.14)	375.60 (0.29)
	376.78 (0.28)	411.33 (1.00)	488.64 (37.60)	528.92 (8.27)
	530.27 (7.98)	550.49 (0.19)	582.78 (0.14)	584.77 (1.30)
	603.29 (211.67)	642.57 (0.10)	643.42 (0.21)	644.18 (64.67)
	664.89 (64.5)	2165.00 (2.95)	2165.22 (8.47)	2170.45 (8.34)
	2170.77 (563.56)	2171.37 (8.45)	2171.70 (581.71)	2175.94 (1805.9)
	2179.91 (1.05)			

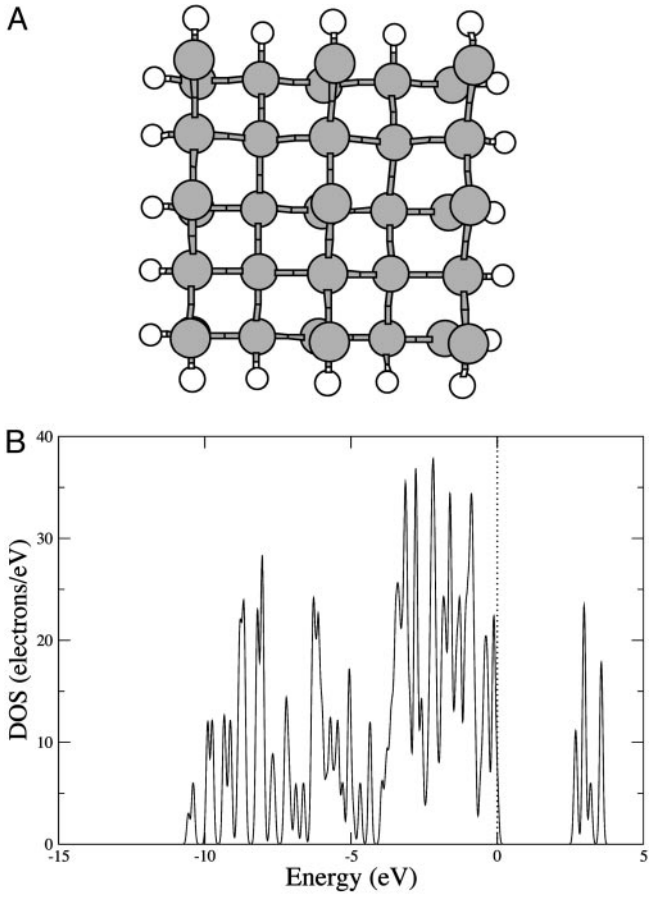

Fig. 4. Electronic band structure of the 3 × 3 1D silicon nanowire (defined as in ref. 32), with the dangling bonds terminated by H atoms (white spheres).

achieve zero-pressure condition in the axial z direction. To study the square, pentagonal, and hexagonal SWSNTs, the supercell contains 8, 10, and 12 Si atoms, respectively. The energy convergence criterion for geometry relaxation is 5×10^{-6} eV per atom. It is found that the optimized value of L_z is 4.77 Å for the square, 4.78 Å for the pentagonal, and 4.79 Å for the hexagonal SWSNTs. As mentioned above, these L_z values represent twice the lattice constant in the axial direction. The calculated energy per atom is −107.934 eV (hexagonal SWSNT), −107.959 eV (pentagonal SWSNT), and −107.803 eV (square SWSNT). The pentagonal SWSNT seems to be the more stable 1D allotrope among the three. We also calculated the energy per atom for the cubic diamond silicon, which is −108.685 eV, and that for a silicon dimer, which is −105.536 eV. Clearly, compared to the bulk silicon, all SWSNTs are metastable allotropes in vacuum.

Fig. 3 *A* and *B* show the calculated band structure and density of states (DOS) of the hexagonal SWSNT. It can be seen that the conduction band is slightly overlapped with the valence band, which indicates that the band gap of the hexagonal SWSNT is zero. That the DOS is nonzero at the Fermi energy (Fig. 3*B*) is also consistent with the zero-gap characteristic of the hexagonal SWSNT. Similar electronic band features have been observed for the pentagonal and square SWSNTs. Thus, the *ab initio* calculations suggest that all three SWSNTs are possibly metals. In contrast, for H-terminated 1D silicon nanowires, previous *ab initio* calculations (30–34) have shown that they possess wider band gap than that (1.17 eV) of cubic diamond silicon. The narrower the silicon nanowires, the wider their band gap. To confirm this 1D quantum-confinement behavior, we used the same plane-wave-based DFT with the same approximation

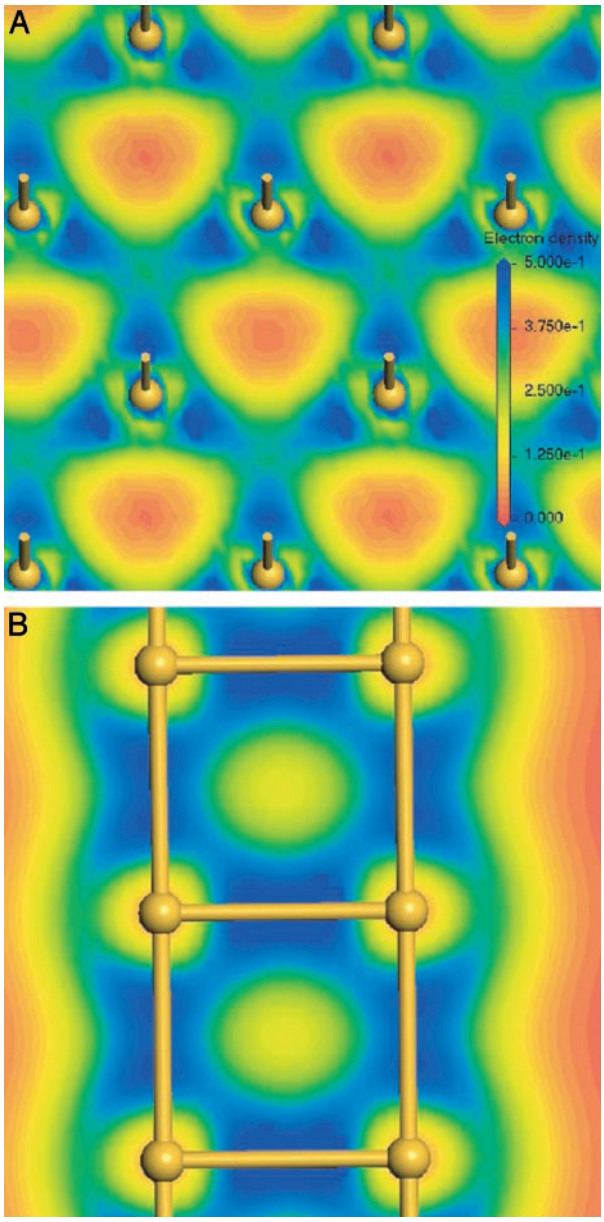

Fig. 5. Electron-density distribution (eV/Å^3) within the (111) plane of the diamond silicon (*A*) and within one of six side planes of the hexagonal SWSNT (*B*). The zero electron density is highlighted by red. The gold-colored spheres denote Si atoms.

(Perdew–Wang generalized gradient approximation) to calculate the band gap of a 3 × 3 silicon nanowire having a width of 7.7 Å (see Fig. 4*A*). Indeed, the calculated band gap is 2.5 eV (see Fig. 4*B*), which is in good agreement with the previous study (32). We note that, for the cubic diamond silicon, the same DFT gives a band gap of only 0.753 eV, appreciably smaller than the measured band gap of 1.17 eV. It is known that DFT usually underestimates the band gap of semiconductors and insulators (35). Consequently, our conclusion on the metallic behavior for the SWSNTs should be considered as tentative. Nevertheless, the predicted opposite trend in the band-gap change for the 1D SWSNTs and for the 1D H-terminated silicon nanowires most likely is a valid conclusion.

We attribute the likelihood of metallic characteristics of the SWSNTs to their distinct local geometric structure, which differs from the perfect tetrahedral structure of the cubic diamond

silicon. Fig. 5*A* shows the electron-density distribution within the (111) plane of the cubic diamond silicon, whereas Fig. 5*B* shows the density distribution within one of the six side planes of the hexagonal SWSNT. The zero electron density is highlighted by red. The appearance of numerous red-colored holes in Fig. 5*A* indicates that valence electrons in bulk silicon are localized in between Si atoms (forming the sp^3 bonds). On the other hand, a no-red-colored region can be seen in Fig. 5*B*, indicating that, in the SWSNT, valence electrons are distributed more uniformly in between Si atoms, thereby enhancing the probability of electron conduction in the axial direction.

In conclusion, the present, thinnest 1D SWSNTs may be produced within nanoscale confinement. Because the bulk silicon has a high melting point (1683 K), the confinement walls must be able to stand high temperatures and be inert from chemical attack of molten silicon. *Ab initio* calculations confirm that the SWSNTs are locally stable in vacuum at zero temperature. A unique structural feature of these SWSNTs is that the coordination number of every Si atom is fourfold, which differs from that of single-walled carbon nanotubes. Ultimate confirmation of this type of SWSNT must await experiments.

We thank Professors K.-M. Ho, K. N. Houk, K. Koga, and S. Sastry for valuable discussions. This work is supported by the National Science Foundation, Office of Naval Research, University of Nebraska, Lincoln, research computing facility, Mitsubishi Foundation, and Japan Ministry of Education.

1. Nilius, N., Wallis, T. M. & Ho, W. (2002) *Science* **297,** 1853–1856.
2. Harrison, P. (2000) *Quantum Wells, Wires and Dots: Theoretical and Computational Physics* (Wiley, New York).
3. Iijima, S. (1991) *Nature* **354,** 56–58.
4. Fagan, S. B., Baierle, R. J., Mota, R., da Silva, A. J. R. & Fazzio, A. (2000) *Phys. Rev. B Condens. Matter* **61,** 9994–9996.
5. Chang, K. L. & Cohen, M. L. (1985) *Phys. Rev. B Condens. Matter* **31,** 7819–7826.
6. Cullis, A. G. & Canham, L. T. (1991) *Nature* **353,** 335–338.
7. Ono, T., Saito, H. & Esashi, M. (1997) *Appl. Phys. Lett.* **70,** 1852–1854.
8. Hasunuma, R., Komeda, T., Mukaida, H. & Tokumoto, H. (1997) *J. Vac. Sci. Technol. B* **15,** 1437–1441.
9. Namatsu, H., Horiguchi, S., Nagase, M. & Kurihara, K. (1997) *J. Vac. Sci. Technol. B* **15,** 1688–1696.
10. Morales, A. M. & Leiber, C. M. (1998) *Science* **279,** 208–211.
11. Zhang, Y. F., Tang, Y. H., Wang, N., Yu, D. P., Lee, C. S., Bello, I. & Lee, S. T. (1998) *Appl. Phys. Lett.* **72,** 1835–1837.
12. Ma, D. D., Lee, C. S., Au, F. C., Tong, S. Y. & Lee, S. T. (2003) *Science* **299,** 1874–1877.
13. Zhang, R. Q., Lee, S. T., Law, C.-K., Li, W.-K. & Teo, B. K. (2002) *Chem. Phys. Lett.* **364,** 251–258.
14. Kang, J. W. & Hwang, H. J. (2003) *Nanotechnology* **14,** 402–408.
15. Barnard, A. S. & Russo, S. P. (2003) *J. Phys. Chem. B* **107,** 7577–7581.
16. Stillinger, F. H. & Webber, T. A. (1985) *Phys. Rev. B Condens. Matter* **31,** 5262–5268.
17. Broughton, J. Q. & Li, X. P. (1987) *Phys. Rev. B Condens. Matter* **35,** 9120–9127.
18. Yoo, S., Zeng, X. C. & Morris, J. R. (2004) *J. Chem. Phys.* **120,** 1654–1656.
19. Steele, W. A. (1974) *Interaction of Gases with Solid Surfaces* (Pergamon, Oxford, U.K.).
20. Rapaport, D. C. (1997) *The Art of Molecular Dynamics Simulations* (Cambridge Univ. Press, Cambridge, U.K.).
21. Koga, K., Gao, G. T., Tanaka, H. & Zeng, X. C. (2001) *Nature* **412,** 802–806.
22. Raghavachari, K. & Rohlfing, C. M. (1988) *J. Chem. Phys.* **89,** 2219–2234.
23. Lu, Z.-Y, Wang, C.-Z. & Ho, K.-M. (2000) *Phys. Rev. B Condens. Matter* **61,** 2329–2334.
24. Zhu, X. & Zeng, X. C. (2003) *J. Chem. Phys.* **118,** 3558–3570.
25. Frisch, M. J., Trucks, H. B. Schlegel, H. B., Scuseria, G. E., Robb, M. A., Cheeseman, J. R., Zakrzewski, V. G., Montgomery, Jr., J. A., Stratmann, R. E., Burant, J. C., *et al.* (2002) GAUSSIAN 98 (Gaussian, Inc., Pittsburgh), Version 11.3, Revision A.
26. Perdew, J. P. & Wang, Y. (1992) *Phys. Rev. B Condens. Matter* **45,** 13244–13249.
27. Payne, M. C., Teter, M. P., Allan, D. C., Arias, T. A. & Joannopoulos, J. D. (1992) *Rev. Mod. Phys.* **64,** 1045–1097.
28. Vanderbilt, D. (1990) *Phys. Rev. B Condens. Matter* **41,** 7892–7895.
29. Monkhorst, H. J. & Pack, J. D. (1976) *Phys. Rev. B Condens. Matter* **13,** 5188–5192.
30. Read, A. J., Needs, R. J., Nash, K. J., Canham, L. T., Calcott, P. D. J. & Qteish, A. (1992) *Phys. Rev. Lett.* **69,** 1232–1235.
31. Buda, F., Kohanoff, J. & Parrinello, M. (1992) *Phys. Rev. Lett.* **69,** 1272–1275.
32. Ohno, T., Shiraishi, K. & Ogawa, T. (1992) *Phys. Rev. Lett.* **69,** 2400–2403.
33. Sanders, G. D. & Chang, Y.-C. (1992) *Phys. Rev. B Condens. Matter* **45,** 9202–9213.
34. Yeh, C.-Y., Zhang, S. B. & Zunger A. (1994) *Phys. Rev. B Condens. Matter* **50,** 14405–14415.
35. Hybertsen, M. S. & Louie, S. G. (1985) *Phys. Rev. Lett.* **55,** 1418–1421.